Nanoscale Fracture Mechanics

Steven L. Mielke,[1] Ted Belytschko,[2] and George C. Schatz[1]

[1]Department of Chemistry, and [2]Department of Mechanical Engineering, Northwestern University, Evanston, Illinois 60208;
email: slmielke@chem.northwestern.edu, tedbelytschko@northwestern.edu, schatz@chem.northwestern.edu

Annu. Rev. Phys. Chem. 2007. 58:185–209

First published online as a Review in Advance on October 23, 2006

The *Annual Review of Physical Chemistry* is online at http://physchem.annualreviews.org

This article's doi:
10.1146/annurev.physchem.58.032806.104502

0066-426X/07/0505-0185$20.00

Key Words

oxidative pitting, carbon nanotube fracture, vacancy defects, Stone-Wales defects, plastic deformation, brittle fracture

Abstract

Theoretical calculations on undefected nanoscale materials predict impressive mechanical properties. In this review we summarize the status of experimental efforts to directly measure the fracture strengths of inorganic and carbon nanotubes and discuss possible explanations for the deviations between the predicted and observed values. We also summarize the role of theory in understanding the molecular-level origin of these deviations. In particular, we consider the role of defects such as vacancies, Stone-Wales defects, adatoms and ad-dimers, chemical functionalization, and oxidative pitting.

INTRODUCTION

CNT: carbon nanotube

Biological systems often make extensive use of hierarchical nanostructured architectures to achieve high strength and toughness (1, 2). The development of scanning probe microscopes in the early 1980s and the discovery of ultrastrong, synthesizable nanoscale materials such as carbon nanotubes (CNTs) (3) ignited intense interest in the development and characterization of manmade nanostructures with properties superior to conventional materials. One of the motivating factors is that the predicted Young's modulus and fracture-stress values for undefected nanotubes and nanorods greatly exceed observed values for macroscopic structures constructed from the same materials; this dramatic increase in strength is partially substantiated by the limited experimental data now available. This suggests that substantial improvements in mechanical properties can be achieved if atomically perfect structures can be fabricated on larger length scales. However, important questions arise as to whether perfection can be or has been achieved even at the nanoscale for CNTs and other structures. This review describes recent theory and experiments that have addressed this question, with particular emphasis on factors that reduce the fracture stress of nanoscale materials significantly below that predicted for perfect materials.

We largely confine our attention to CNTs and closely related nanotubes such as those of boron nitride and tungsten disulfide. Many other interesting nanoscale materials have attracted attention for their mechanical properties, but CNTs have attracted particular attention owing to their availability, their accessibility to experimental measurements at the single-tube level, and their accessibility to theoretical study. There is an extensive literature on many other closely related materials that we do not summarize, including scrolled exfoliated graphene sheets (4, 5), exfoliated sheets of graphite oxide (6), ultrananocrystalline diamond (7, 8), various types of nanowires and nanorods (9–11), and metal oxide nanocomposites (12). The study of composites consisting of these materials in a polymer matrix is a subject of great interest in its own right and indeed is likely the most straightforward vehicle by which these nanomaterials will find their way into practical applications, but it is beyond the scope of this review.

THEORETICAL METHODS

We describe the theoretical aspects of nanoscale fracture mechanics first, as these have been extensively studied, and there is now a reasonable understanding of many of the key issues that underlie the role of nanotube structure and defects on mechanical properties. This discussion provides background for the rather confusing state of experimental studies.

The need for detailed modeling of the mechanical properties of nanoscale materials has presented new challenges for theoreticians. For certain deformation modes, such as the bending and buckling of nanotubes (13), continuum methods based on the exponential Cauchy-Born rule (14, 15) provide reasonable results. However, in the study of fracture and defect evolution at this length scale, atomistic simulations are necessary, and quantum effects can be important. Theoretical simulation of fracture

represents a particular challenge because it requires interaction potentials capable of explicitly describing the breaking of chemical bonds. Quantum mechanical (QM) electronic structure calculations provide a natural (and sometimes necessary) way of treating bond fracture, but they remain limited to small systems because of their high computational cost.

QM: quantum mechanical

DFT: density-functional theory

REBO: reactive empirical bond order

Density-functional theory (DFT) methods, with generalized gradient approximation functionals, provide the highest level of accuracy feasible for most QM studies; however, computational effort has limited what can be readily studied to constrained energy minimizations for systems with a few hundred atoms. Semiempirical methods, such as PM3 and AM1, and tight-binding methods often provide a reasonable compromise between accuracy and computational efficiency when larger system sizes need to be considered; for instance, PM3 predicts CNT Young's modulus values to within ~15%, and fracture stresses to within ~20% compared with DFT results (16). Thus, although studies by these methods cannot provide results of high absolute accuracy, they are useful for studying the consequences of various changes in structure.

The use of multiscale methods employing molecular mechanical (MM) treatments (e.g., QM/MM) can extend the sizes of feasible models, although their usefulness depends on the suitability and accuracy of empirical potentials for the phenomena studied. Indeed, many studies can only be done with empirical potentials, or with empirical potentials coupled to continuum mechanics (17–19). Larger models are essential in the study of defects because the distortion in the electronic structure and the deformation field extend far beyond the immediate vicinity of the defect. Application of periodic boundary or prescribed displacement boundary conditions in the vicinity of a defect often leads to incorrect calculations of their effects.

Using the concepts of bond order in chemical systems originally explored by Abell (20), Tersoff (21, 22) developed a methodology for creating empirical bond-order potentials for modeling chemical reactions. Brenner and coworkers (23–25) revised and extended these reactive empirical bond-order (REBO) potentials, and their availability has enabled a vast number of calculations on carbon-based systems.

One serious limitation of these potentials in fracture studies is the use of cutoff functions that restrict interactions to nearest neighbors. When cutoff functions are activated at interatomic distances that are important in describing the fracture process, spuriously high bond forces are generated, leading to highly erroneous results. A partial circumvention of this problem is available (26, 27) that generates reasonable results for regimes in which new bond formation is not important, but inattention to this complication continues to render many theoretical simulations unreliable. Development of new reactive potentials (28–32) remains an area of active interest.

Nuances also exist at the QM level for the accurate treatment of CNTs, and these complications are often underappreciated. One example concerns the Peierls distortions (33, 34) observed for finite-sized CNTs. These lead to substantial bond alternation effects and variations in reaction energies as a function of position along the tube axis. For theoretical fracture studies, Peierls distortions can also lead to multiple fracture pathways (16). Another common complication involves the boundary effects associated with the use of small QM subdomains in QM/MM calculations

SWCNT: single-walled carbon nanotube

MWCNT: multiwalled carbon nanotube

employing link-atom schemes. Because the bond order at the hydrogen-terminated boundary has to be 1, the remaining two bonds need to have an average bond order of 1.5 (a substantial deviation from the mean bond order of 4/3), and this affects the bonding further inside the subdomain. This boundary effect can seriously alter the properties of small QM subdomains; in some cases, this is so severe that higher-level QM corrections with small subdomains in multilevel schemes can be worse than just a single-level calculation with a lower-level theory. [See the work of Chen et al. (35) for a careful study of this concern.]

Undefected Carbon Nanotubes

We begin this section by considering the structural and mechanical properties of undefected CNTs.

Structural properties. We may consider the body of a CNT as a rolled graphene sheet. In particular, a chiral vector (3)

$$\mathbf{C_h} = n\mathbf{a}_1 + m\mathbf{a}_2 \equiv [n, m]; \quad 0 \le |m| \le n, \tag{1}$$

where n and m are integers, and $\mathbf{a}_1$ and $\mathbf{a}_2$ are the lattice vectors, defines the rolling direction. The diameter is given by

$$d = \frac{1}{\pi}\sqrt{\mathbf{C_h} \cdot \mathbf{C_h}} = \frac{\sqrt{3}d_{C-C}}{\pi}\sqrt{n^2 + nm + m^2}, \tag{2}$$

where d_{C-C} is the carbon-carbon bond distance. (In graphene this is ~1.42 Å, but for small-diameter CNTs this tends to be closer to 1.44 Å.) The chiral angle (i.e., the angle between $\mathbf{C_h}$ and $\mathbf{a}_1$) is defined by

$$\cos\theta = \frac{\mathbf{C_h} \cdot \mathbf{a}_1}{|\mathbf{C_h}|\,|\mathbf{a}_1|} = \frac{2n + m}{2\sqrt{n^2 + m^2 + nm}}. \tag{3}$$

Armchair tubes correspond to $n = m$ (and thus have $\theta = 30^\circ$), zigzag tubes correspond to $m = 0$ (and thus have $\theta = 0^\circ$), and chiral tubes correspond to cases where $0^\circ < \theta < 30^\circ$.

The ends of CNTs may be open, but more typically they are closed by caps. Such caps involve a mixture of five- and six-membered rings; when regularly shaped, the caps resemble a hemisphere of a fullerene and possess at least six isolated pentagons. The five-membered rings of the end caps are substantially more reactive than the CNT sidewalls; this allows the ends to be preferentially functionalized or even opened so the tubes may serve as molecular containers. CNTs have been filled with a wide variety of substances; such applications are too numerous to survey here, but as one example of how readily this occurs we note that single-walled carbon nanotubes (SWCNTs) placed in molten iodine (36) open at the ends and are filled by a pair of helical chains of iodine atoms that span the length of the tube.

The first CNTs discovered (37), which were obtained by an arc-discharge vaporization procedure, were multiwalled carbon nanotubes (MWCNTs); i.e., they consisted of a number of concentric shells with a typical interlayer spacing of ~0.34 nm.

Subsequently, synthetic methods employing catalytic metal particles were discovered that produced SWCNTs; a vast number of such methods have been published, but perhaps the first such process used to produce commercial quantities of product was the high-pressure CO conversion (HiPCO) process of Nikolaev et al. (38). Synthetic methods (39) that produce predominantly double-walled carbon nanotubes (DWCNTs) have also been developed; these tubes exhibit some improved properties compared with SWCNTs, including greater thermal stability (40) and resistance to oxidation (41). Most CNT syntheses yield tangled and disordered bundles or ropes of tubes; however, some procedures have been presented that produce either aligned bundles (39, 42, 43) or isolated (44) tubes.

DWCNT: double-walled carbon nanotube

Isolated SWCNTs with a diameter larger than ~60 Å may exist in a cylindrical shape, but it is energetically favorable for these tubes to collapse into ribbon structures (45, 46). For SWCNTs with diameters between ~24 Å and ~60 Å, a ribbon structure is possible but the cylindrical structure is energetically favorable, and for diameters less than ~24 Å, only the cylindrical structure is stable. For MWCNTs the diameter range for which ribbon structures are stable is shifted to larger values, whereas bundles of SWCNTs have stable ribbon structures for lower diameter values than observed for isolated tubes (46).

Mechanical properties. Several QM calculations have been presented for the fracture strength of pristine (undefected) CNTs (16, 47–50). The DFT results (16, 47) indicate that a [10, 0] tube has a failure stress of ~105 GPa at ~20% strain, whereas a [5, 5] tube has a failure stress of ~110 GPa at ~30% strain. Lower-level calculations (19) suggest that both the failure strains and failure stresses of chiral tubes increase monotonically with the chiral angle θ and are nearly independent of diameter except at very small sizes. Calculated Young's moduli tend to cluster around 1.0 TPa, and reasonable estimates (51, 52) of the Poisson ratio cluster around 0.15.

Inorganic Nanotubes

Numerous inorganic variants of nanotubes have been prepared, with boron nitride (BN) (53), tungsten disulfide (WS_2) (54, 55), and molybdenum disulfide (MoS_2) (56, 57) among those that have received considerable attention for their mechanical properties. BN nanotubes are structurally similar to CNTs, with the body consisting of hexagons comprising alternating B and N atoms, except the curvature of the end caps is believed (58) to be introduced via four- and eight-membered rings rather than the five-membered rings observed in CNTs because odd-membered rings need to contain relatively unfavorable B–B or N-N bonds instead of only B-N bonds. Indeed, these two nanotubes are so similar that multiwalled nanotubes consisting of a mix of BN and carbon shells have been produced (59); these are sometimes referred to as BCN nanotubes. BN nanotubes may be synthesized directly or be produced by selectively oxidizing the carbon layers of BCN nanotubes (60), or by a substitution reaction (61) that transforms CNTs into BN nanotubes. Chen et al. (62) have recently proposed a purification regimen for BN nanotubes.

TEM: transmission electron microscope

WS_2 nanotubes (the structure of various other AB_2 nanotubes such as MoS_2 and SiO_2 is similar) involve tungsten atoms tetrahedrally bonded to four sulfur atoms; when unrolled, a WS_2 nanotube yields a layered structure with a sheet of tungsten atoms sandwiched between two sheets of sulfur atoms; the interlayer spacing in WS_2 is ~0.615 nm. Seifert et al. (57) have modeled square-like and octahedral-like defects that permit the formation of end caps in these materials.

BEYOND PERFECT STRUCTURES

The lowest energy defect in a CNT is the Stone-Wales (SW) defect (63), i.e., the result of a 90° rotation of a C–C bond pair (referred to as an SW transformation) that transforms four hexagon rings into two pentagons and two heptagons (often denoted as a 5/7/7/5 defect). QM calculations (64, 65) have shown that an SW transformation becomes energetically favorable above strains of ~5% in armchair CNTs and above ~12% in zigzag CNTs (66). A subsequent SW transformation adjacent to an extant SW defect may result in the bifurcation of the SW defect into two separated pentagon-heptagon (5/7) pairs, and additional SW transformations cause these 5/7 defects to migrate along the tube; such defect migration can change the chirality of the CNT (64, 67). Splitting of SW defects has been shown to be energetically favorable for low strains, whereas aggregation of SW defects is favorable at higher strains (68). Hasimoto et al. (69) claim to have imaged directly an isolated 5/7 defect in an SWCNT using a high-resolution transmission electron microscope (TEM).

Yakobson (67) has argued that aggregation of SW defects can be followed by a ring-opening mechanism, leading to the nucleation of a crack and the ultimate failure of the tube. Yakobson and coworkers (70–72) have on a number of occasions presented primitive rate-theory estimates for CNT failure based on the assumption that once SW defects begin to form at a reasonable rate, CNT failure by this aggregation and cracking mechanism follows precipitously. SW transformations also occur in BN nanotubes (73, 74), and Dumitrica & Yakobson (75) have proposed rate theories for their fracture that are similar to those for CNTs. We note that in BN nanotubes the final structure depends on the direction of an SW rotation, and the transformation results in relatively unfavorable B–B and N-N bonds.

MD simulations of CNT fracture (76, 77), using REBO potentials and conducted at very high temperatures (for reasons of computational efficiency), have displayed substantial weakening resulting from stress-induced SW defects and have thus provided seeming support for this proposed failure mechanism. However, calculations by Troya et al. (49) on CNTs displaying multiple, aggregated SW defects indicate that, quantum mechanically, the bond between the pentagon rings of an SW defect is stronger than a typical C–C bond, and failure instead proceeds via fracture of other bonds within the pentagon and/or octagon rings—even when this requires fracturing twice as many bonds. Failure stresses and strains were only modestly below those observed for pristine tubes. Troya et al. (49) also showed that fracture studies with REBO potentials erroneously predicted that the C–C bonds between pentagon rings in SW defect aggregations were weak and led to fracture at substantially reduced stresses and strains. Thus, the failure mechanisms observed in the MD simulations

are partly an artifact of the inaccurate empirical potentials employed. The remarkable strength of the bond connecting the two pentagons in an SW defect has not been fully appreciated in other contexts; Bettinger (78) remarks that many studies on the chemical reactivity of SW defect sites only focus on this bond, whereas the weaker bonds are usually the most appropriate point of chemical attack.

The barriers to SW transformations (65) remain prohibitively high at strains well above those at which the defect, and aggregation of extant defects, is energetically favorable. Belytschko and coworkers (27, 50) have argued that CNT fracture, at least at room temperatures, proceeds via brittle failure mechanisms. Ewels et al. (79) and Jensen et al. (80) have discussed how carbon adatoms lower the barrier to SW transformations by a factor of ~3–5 and point out that boron adatoms are even more effective at this barrier lowering. This effect of adatoms may enhance the rate of removal (a second SW transformation at the location of an extant SW defect returns the tube to a pristine condition and is energetically favorable at low strains) or bifurcation of SW defects during the synthesis and annealing steps. Orlikowski et al. (81, 82) and Sternberg et al. (83) have considered reactions of ad-dimers to CNTs. These can result in local expansion of the circumference of the tube or the addition of isolated defects involving two 5/7 defect pairs oriented so that the pentagons share a side (which can be denoted a 7/5/5/7 defect) and the heptagon rings are separated by a C–C bond. Orlikowski et al. (81, 82) point out that subsequent separation of these two dislocation pairs leads to a plastic deformation mode that is distinct from that involving stress-induced SW transformations and that can lead to localized regions of altered helicity.

Vacancy defects in graphene and CNTs have received considerable attention (16, 84–91). Such defects can be readily induced in graphitic materials by high-energy electron irradiation (92) that can displace carbon atoms from the lattice. Such knock-out events may also lead to interstitial defects (87, 88). Few-atom vacancy defects can readily reconstruct by the formation of five-membered rings; one-atom vacancies result in one pentagon ring and a dangling bond, whereas two-atom vacancies lead to two pentagons and an octagon without any dangling bonds. Isolated CNTs subjected to heavy irradiation can reorganize into smaller-diameter, albeit highly defective, CNTs (85). Electron irradiation can also be used to weld CNTs, and in certain cases it can cause two CNTs to coalesce (93). Kis et al. (88) have used electron irradiation to create bridging defects in SWCNT bundles, resulting in a 30-fold increase in the bending modulus and enhancement of other mechanical properties; irradiation might also prove useful in increasing load transfer to inner shells in MWCNTs. Vacancy defects have also been extensively studied in BN nanotubes (94, 95).

One- and two-atom vacancies were shown to reduce CNT fracture strength by as much as 26% (16, 19). However, the most deleterious effect of vacancies might be their tendency to serve as nucleation sites for oxidative pitting that can result in the evolution of large holes (16, 19, 96–99). Other large-scale defects are also of potential concern, including unremoved catalyst particles and cracks.

Chemical functionalization of CNTs may occur inadvertently during purification processes and is intentionally used to improve solubility, and thereby aid in dispersal, or to enhance interactions with polymers when the tubes are intended for use as

fiber reinforcements. Chemical functionalization (78, 100, 101) occurs preferentially at end caps, defect sites, the edges of collapsed tubes [which provides a means for pressure-induced functionalization (102)], and, in general, at any area subject to local stress or distortion, thus providing opportunities for mechanically induced chemistry (103) and diameter selectivity (104). Even the pristine sidewalls may be readily functionalized under appropriate conditions, including acid and/or oxidation treatments (105), gas-phase fluorination (106–108) (which has been shown to readily functionalize CNTs with decoration densities approaching 50%), and plasma treatments to achieve hydrogenation (109) or fluorination (110, 111). Extensive functionalization may alter the mechanical properties of CNTs; however, it does not necessarily have to dramatically alter the fracture strength: Fracture studies (D. Troya, S.L. Mielke & G.C. Schatz, unpublished calculations) on fluorinated CNTs with coverages as high as 50% displayed fracture strength reductions of only ~25–50%, with the upper range observed only when an entire line of sp^3-sp^3 hybridized C–C bonds lies perpendicular to the tube axis.

EXPERIMENTAL FRACTURE STUDIES

The mechanical properties of CNTs depend on both the synthetic scheme and the purification procedures (112–116) used in their preparation because these influence the types and concentrations of defects introduced, the presence of impurities, the diameter distribution, the number of shells (for MWCNTs), and so on. After the initial preparation, the reaction product may be contaminated by catalyst particles and by amorphous carbon, undesired or defected nanoparticles, and soot. Most purification schemes employ some form of oxidative-etching process to remove the bulk of the soot and highly defected nanoparticles; an exception is the scheme of Vivekchand et al. (117) that involves reduction with H_2. It is usually necessary to remove any catalyst particles—typically achieved via acid washes (these may need to be preceded by a preliminary, mild, low-temperature oxidative etch to remove some of the soot encrusting the catalyst particles)—prior to this oxidative etching, or the metal particles will catalyze rapid oxidation of the desirable nanoparticles. Unfortunately, oxidative etching can dramatically increase the size of small defects present in nearly perfect specimens. For example, oxidative pitting of graphite (96–99) initiated at vacancy defect sites and resulting in large roughly circular holes in the surface graphene sheet has been well studied, and similar pitting will occur in CNTs. Annealing CNTs at high temperatures serves to remove some defects and provides enhanced stability versus oxidation (118).

Sonication is often used to aid in the dispersal of CNTs; however, this results in local hot spots (cavitation bubbles) that may result in enhanced susceptibility to chemical attack and introduce new defects or enlarge pre-existing ones. For instance, studies have shown that even dilute nitric acid can dramatically damage CNTs at elevated temperatures (119).

Much of the early fracture work involved bundles of nanotubes, and we summarize these first. In a few instances, experimental results for the fracture of isolated MWCNTs are available, and we discuss these next. Perhaps the most generally

desired measurement—the fracture strength of high-quality isolated SWCNTs—has thus far proven elusive, but some initial, tentative studies of SWCNTs are being conducted.

AFM: atomic force microscope

SEM: scanning electron microscope

EBID: electron-beam-induced deposition

Fracture Studies of Carbon Nanotube Bundles

Wagner et al. (120) studied the fracture of arc-discharge synthesized MWCNTs embedded in a polymer matrix film placed under tension. The matrix, which had a modulus of 2 GPa, displayed a failure stress of 60 MPa, and the nanotubes embedded perpendicular to the straining direction displayed multiple fractures. Using a simple isostrain model, the authors estimated the fracture stress of the MWCNTs was ~55 GPa if they assumed the CNT's modulus was 1.8 TPa; using a more up-to-date modulus estimate of 1.0 TPa would yield a failure stress estimate of ~31 GPa.

Pan et al. (121) studied the fracture of ropes of MWCNTs synthesized by pyrolysis of acetylene over iron/silica substrates (42). Ten samples, with diameters ranging from 10 to 50 μm, were mounted in a stress-strain puller with epoxy glue and loaded tensilely until failure. The mean values observed for the Young's modulus and fracture stress were 0.45 ± 0.23 TPa and 1.72 ± 0.64 GPa, respectively.

Walters et al. (122) reported fracture studies on four SWCNT bundles synthesized by the procedure of Thess et al. (123) and purified by the procedure of Rinzler et al. (114). The bundles were pinned to opposites sides of a trench and prodded laterally with an atomic force microscope (AFM) tip until failure occurred. The failure strains were then estimated, based on the observed force on the AFM tip prior to failure, as 2.8 ± 0.4%, 5.8 ± 0.9%, 1.2 ± 0.2%, and 1.1 ± 0.1%. Based on these measurements, the authors suggested that a lower limit on the failure strain of an isolated SWCNT was 5.8 ± 0.9%.

Yu et al. (124) reported fracture studies on 15 SWCNT bundles, with diameters ranging from 19 to 41 nm, produced by a laser ablation method and purified by the procedure of Rinzler et al. (114). A tangled mass of SWCNT bundles (referred to as SWCNT paper) was torn so that a few isolated bundles projected out from the tear edge. The authors placed this mass inside a scanning electron microscope (SEM) and attached an AFM cantilever to one of the projecting ropes via an electron-beam-induced deposition (EBID) process (125), and the bundle was then tensilely loaded until failure. The observed failure stresses, assuming all tubes in the bundle were uniformly loaded, ranged from 3 to 11 GPa, and the mean fracture strength was 6.7 GPa. In eight of the 15 tests, it was possible to measure the strain; in these, the failure strains ranged from 1.1 to 5.3%, and the Young's modulus (again assuming equal load distribution) ranged from 140 to 280 GPa. If, instead, only the outer fringe of the bundle was assumed to be load bearing, the reported fracture strengths ranged from 16 to 52 GPa, with a mean value of 30 GPa, and the reported Young's moduli ranged from 320 to 1470 GPa, with a mean value of 1000 GPa.

Li et al. (126) took aligned SWCNT bundles synthesized by catalytic hydrocarbon decomposition (127) and impregnated them with polyvinyl chloride to form a composite. Six of these samples were then loaded to failure tensilely, and the fracture strengths of the SWCNT bundles were estimated from the fracture strengths of the

composites based on the rule of mixtures. The estimated fracture strength of the bundles ranged from 2.3 to 14.2 GPa, with a mean value of 7.5 GPa; assuming that the volume fraction of SWCNTs within the bundles was 65%, the fracture strength of isolated SWCNTs was estimated as ranging from 3.6 GPa to 22.2 GPa, with a mean value of 11.5 GPa.

Cooper et al. (128) embedded SWCNT bundles in an epoxy resin film and searched for samples in which the bundles spanned a void in the film. Three such bundles (having diameters of 15.6, 16.2, and 11.5 nm) were fractured by lateral prodding with an AFM tip, and the resulting failure stresses were determined to be 277 ± 50, 42 ± 5, and 114 ± 50 GPa, respectively. They applied similar procedures to a fourth SWCNT bundle and six embedded MWCNTs; all resulted in pullout of the nanotube from the matrix, which allowed the authors to also measure shear strengths for the nanotube-polymer interface.

Li et al. (129) reported eight measurements for the fracture of bundles of DWCNTs obtained by catalytic chemical vapor deposition (CVD) with a xylene feedstock (39); these bundles are estimated to consist of more than 80% DWCNTs (having a typical diameter of ~2 nm), with the remaining tubes being mainly single or triple walled. Strands comprising large numbers of DWCNT bundles and having diameters of ~3–15 μm were glued with epoxy onto a stress-strain puller and loaded until failure. The strands failed at strains of 3.5%–13.2% (average 9.0%), and the mean values of the observed Young's moduli and failure stresses were 16 and 1.2 GPa, respectively. Assuming that the bundles composed approximately 20% of the volume of the strands, the authors estimated the moduli and failure stresses of the DWCNTs bundles as 80 and 6 GPa, respectively.

Considerable recent effort has been directed toward producing macroscopic yarns composed entirely of nanotubes (130–132). Ericson et al. (132) have reported yarns of SWCNTs that have a Young's modulus of 120 GPa and a tensile strength of 116 MPa, whereas Zhang et al. (131) have reported a tensile strength of 460 MPa for yarns of MWCNTs.

Fracture Studies on Isolated Multiwalled Nanotubes

Yu et al. (133) conducted the first fracture study on isolated CNTs by measuring the mechanical properties of 19 arc-discharge-grown (134) MWCNTs by tensile loading between AFM cantilevers within an SEM. The tubes were fixed to the cantilevers using an EBID process. The fracture strengths ranged from 11 to 63 GPa, with a mean value of 28 GPa; **Figure 1*a*** shows a plot of the observed fracture strengths as a function of the outer tube diameter. Strain data were available for four tubes, and the strains at failure ranged from 2 to 13%, whereas the observed Young's modulus ranged from 0.27 to 0.95 TPa. Only the outer shell proved to be load bearing, and after this layer fractured, the interior layers were pulled out in what has been termed a sword-in-sheath failure mode (133, 135). After fracture, the tubes were examined in a TEM, and some of the outer shells were observed to have collapsed into ribbons.

The modulus values reported by Yu et al. (133) are anomalously low compared with the expected graphitic modulus of ~1 TPa. It has been speculated (27) that this may

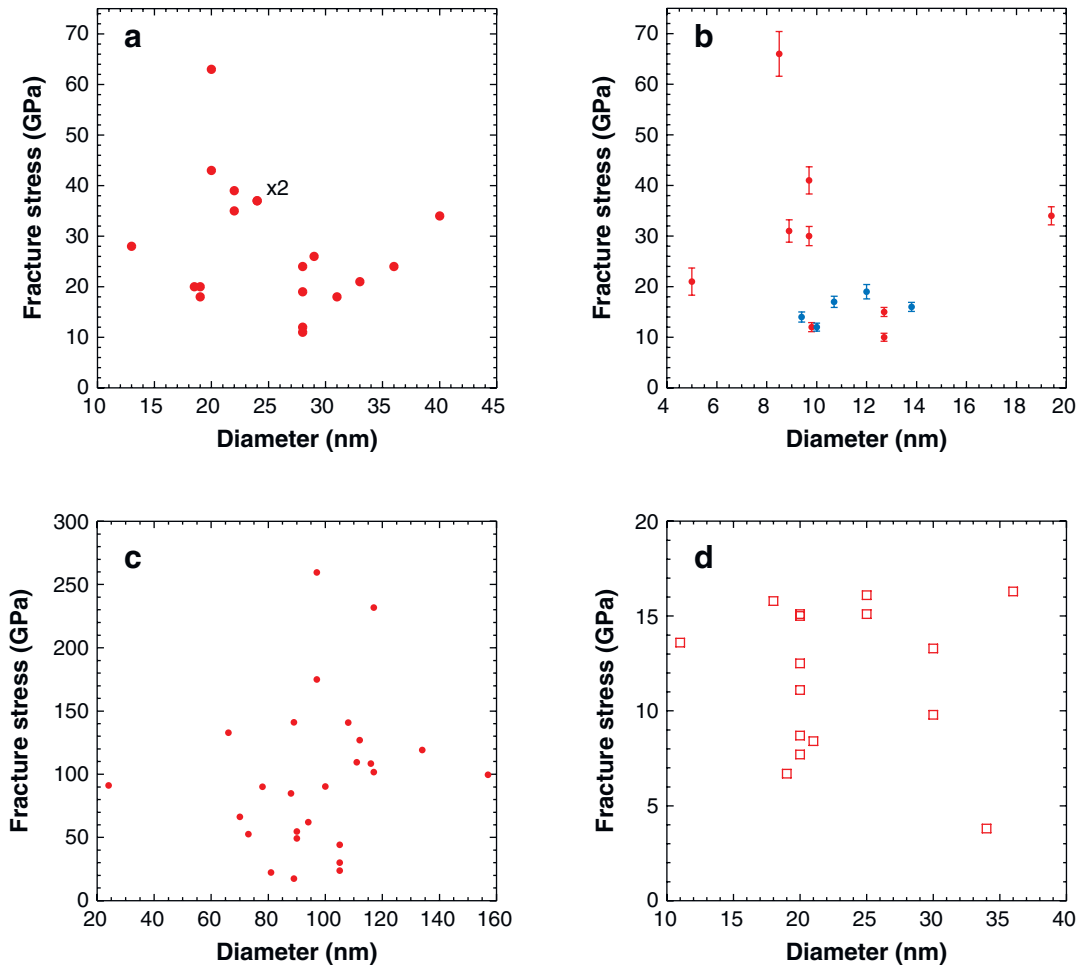

Figure 1

Distribution of fracture strengths versus the outer tube diameter for various nanotube fracture experiments. (*a*) Multiwalled carbon nanotube (MWCNT) fracture experiment of Yu et al. (133). (*b*) MWCNT fracture experiment of Ding et al. (139). (*c*) MWCNT fracture experiment of Barber et al. (140). (*d*) WS_2 nanotube fracture experiment of Kaplin-Ashiri et al. (142).

have resulted from slippage of the CNTs at the cantilever tips; if this indeed occurred, the modulus and failure-strain values must be regarded as only lower and upper bounds, respectively, on the true values. However, the failure stress measurements would not have been affected by this complication. The observed failure stresses, although impressive, are still significantly below the peak strengths anticipated by theory for pristine CNTs and display a large variance. Mielke et al. (16) suggested that holes were introduced by the purification procedure (134) used on the tubes, which involved oxidative etching in air at 650°C for 30 min, followed by acid baths and

annealing. Theoretical calculations (16, 19) indicate that modest-sized and roughly circular holes result in significant strength reductions sufficient to reproduce the observed range of fracture strengths. Extensive oxidative pitting, sufficient to remove ~25% of the outer shell, would likely reduce the Young's modulus to within the experimentally observed range.

Demczyk et al. (136) reported the fracture of a single 12.5-nm diameter MWCNT synthesized (137) by an arc-discharge method that resulted in boron doping of 1%–5%. This tube, which contained an estimated 13 layers, was mounted on a tensile-testing device contained within a TEM; adhesion between the tube and a gold surface film held the tube fixed at both ends. Demczyk et al. (136) reported a modulus of 0.91 TPa, a failure strain of 5 ± 2%, and a failure stress of 150 ± 45 GPa under the assumption that only the outer tube was load bearing. However, a failure stress of this size is not consistent with the relatively low failure strain observed unless there was significant interlayer load transfer. One possible explanation for this is that bridging defects (87, 88) were introduced by irradiation from the high-energy TEM imaging used to monitor the fracture. Another possibility is that the boron impurities facilitated bridging between the concentric layers of the tube—boron interstitials have induced welding of CNTs in other circumstances (138).

Ding et al. (139) measured the fracture strength of 14 arc-discharge-grown MWCNTs, using the same loading procedure as Yu et al. (133). To obtain a few suitable tubes, the authors sonicated the unpurified MWCNT-containing product in ethanol to separate some tubes from the soot; for nine measurements, the tubes were sonicated for 12 h, whereas for the remaining five measurements, the tubes were sonicated for only 10 s. The Young's modulus measurements ranged from 620 ± 85 to 1200 ± 250 GPa, with a mean value of 955 GPa, and the stress-strain curves appear roughly linear, lacking the irregular steps of earlier experiments (124, 133). This mean value for the modulus is in good agreement with the theoretical predictions and is in marked contrast to the very low values of the earlier MWCNT fracture experiment (133). The failure strains for the 14 tubes ranged from 1.0 ± 0.2% to 6.3 ± 0.5%, with a mean of 2.6%; in all cases the tubes failed by a sword-in-sheath mode. Only in four of the 14 instances did the failure strain exceed 3.0%. Yu et al. (133) only reported failure-strain data for four tubes, but three of these were in excess of 10%. The fracture stresses ranged from 10 ± 0.8 GPa to 66 ± 4 GPa with a mean value of 24 GPa, a range comparable with the earlier Yu et al. (133) results. **Figure 1*b*** gives a plot of the fracture strengths versus the outer tube diameter; the data for tubes treated with long and short sonication times are given different colored symbols.

The fracture strengths for the tubes sonicated for the short time interval are significantly lower than those for the tubes sonicated for longer times. (The means are 15.6 and 28.9 GPa, respectively.) This observation is consistent with the expectation that extensive sonication enlarges existing defects and possibly even introduces additional defects where none previously existed. However, it also suggests that sonication may have the beneficial effect of completely fracturing tubes at the sites of very large defects (thus, effectively removing some catastrophic defects) and that under some conditions this effect is more significant than the weakening effect of enlarging

defects without causing complete fracture. It would be interesting to explore further what the optimal degree of sonication is.

Curiously, for two of the 14 fracture measurements of Ding et al. (139), the stress-strain curve suddenly flattens out (i.e., the strain increases dramatically while the stress remains roughly constant), thus suggesting that some form of plastic yielding was observed. These transitions occurred at strains of 2.7% and 4.7%, and extensions were observed until beyond strains of 8% and 17%, respectively. The employed loading scheme in this as well as the earlier Yu et al. (133) experiment involves tensile loading at an approximately constant stress rate; consequently, during plastic failure large (∼5%) strain steps are taken, and such failure modes can easily be missed. For the first tube in which this failure mode was observed, only a single additional strain step was obtained; for the second such tube, only two additional steps were observed. A plausible explanation for such a plastic failure mode is not readily apparent; for instance, the observed onset strains are well below those at which SW transformations become energetically favorable.

Barber et al. (140, 141) reported fracture measurements on 26 CVD-grown (43) MWCNTs via tensile loading with cantilevers within an SEM in a procedure similar to that used by Yu et al. (133), except the tubes were mounted to the cantilevers with an epoxy glue rather than an EBID process. The outer diameters of these tubes ranged from 66 to 157 nm—substantially larger than the arc-discharge MWCNTs studied by Yu et al. (133) and Ding et al. (139). The fracture strengths were reported to range from 17.4 to 259.7 GPa, with a mean value of 97 GPa; **Figure 1*c*** presents a plot of the fracture strengths as a function of the tube diameter. This average strength estimate is superficially in good agreement with the theoretically predicted fracture strengths, but the one reported fracture strain of ∼5% indicates that this is the result of substantial load transfer to layers beneath the outer shell rather than maximal extension of a single shell. Most of these tubes were reported to fracture with a clean break (i.e., with all layers broken rather than via the sword-in-sheath failure mechanism reported for arc-discharge-grown MWCNTs). The authors point out that the CVD-grown nanotubes possess highly irregular wall structures compared with the arc-discharge-grown nanotubes, and suggest this makes it difficult for the outer shells to slip past the inner ones, thus facilitating substantial load transfer between layers.

Kaplan-Ashiri et al. (142) reported 16 fracture-strength measurements (see **Figure 1*d***) on multiwalled WS_2 nanotubes synthesized by the procedure of Tenne et al. (54). The fracture strengths ranged from 3.8 to 16.3 GPa, with a mean value of 11.8 GPa; all tubes failed via a sword-in-sheath failure mode, suggesting that only the outer layer is load bearing. In 10 of the 16 tests, strain data were available. The Young's modulus (based on a shell-thickness parameter of 6.2 Å) measurements ranged from 82 to 218 GPa, with a mean value of 152 GPa, which can be compared with an earlier experimental estimate of 172 GPa (143). The failure strains ranged from 5.0 to 14.0% with a mean value of 9.6%.

Hong et al. (144) have reported a simple procedure for extracting inner shells from small-diameter CVD-grown (145) MWCNTs. The process begins by placing an isolated MWCNT on an SiO_2 substrate and prodding the tube laterally until

fracture occurs and the inner shells begin to be extracted. As these inner shells extend out onto the substrate, friction increases until a subsequent shell fracture occurs. Interestingly, such fractures tend most often to involve pairs of shells, presumably because the deformation of the tubes owing to contact with the surface significantly increases the interactions between the two outermost shells. Occasionally a single outer shell fractures, but in such cases a subsequent fracture occurs after only modest further extrusion, suggesting that frictional forces between an MWCNT and a single shell in contact with the substrate are substantially higher than if the MWCNT was separated from the surface by a double shell. It would be interesting to use this process to shuck the outermost layers—which presumably are most subject to purification-induced defects—prior to mechanical measurements on MWCNTs.

SINGLE-WALLED CARBON NANOTUBE EXPERIMENTS

SWCNTs have been created in situ within a TEM by the irradiation of an amorphous carbon film (146). Irradiation of a film containing two closely spaced holes resulted in progressive widening of the holes and the transformation of the intervening wall initially into a carbon fiber and subsequently into an SWCNT. Further irradiation caused the coalesced hole to widen still further, thus placing the straddling SWCNT under tension. Eventually, the nanotube underwent substantial necking—down to a diameter of ~0.3 nm, which the authors suggest corresponds to a [4,0] CNT. Ajayan et al. (85) have modeled the reconstruction of SWCNTs under irradiation, and they observed facile diameter changes in the simulation. The irradiated 0.3-nm diameter nanotube elongated by as much as 50% before it transformed into a single chain of carbon atoms and eventually fractured completely. Yakobson et al. (147) have observed the formation of such carbon strings in high-strain-rate MD simulations of nanotube fracture.

Bozovic et al. (148) have reported that local plastic deformation of SWCNTs may be achieved by lateral prodding of clamped nanotubes laid on an SiO_2 surface by conductive AFM tips having applied voltages of ~10 V. In particular, permanent deformations corresponding to ~30% local strains were induced in tubes that were globally strained to less than 1% by the action of the AFM tip.

Huang et al. (149) have reported the in situ creation of SWCNTs by the electrical breakdown of MWCNTs inside a TEM equipped with a piezo manipulator that was then used to tensilely strain the SWCNTs to failure. These authors indicate that at room temperature, such SWCNTs typically fail at strains of less than 15%, but if a bias voltage of 2.3 V is applied to an SWCNT—which is sufficient to raise a tube's temperature to above 2000°C—the tube undergoes superplastic deformation to strains of ~280% while undergoing a 15-fold reduction in diameter (from ~12 nm to 0.8 nm). At such elevated temperatures, bifurcation of SW defects and 7/5/5/7 defects into isolated pairs of 5/7 defects (64, 67, 68, 81, 82) or double vacancies into isolated pairs of single vacancies (85) and other such processes can rapidly transform SWCNTs into lower-diameter tubes. Apparently, at very high temperatures, such processes are sufficiently fast that these reorganizations occur before substantial stresses can be applied—at least at the strain rates employed in the experiment. At these

temperatures, the tubes may also be expected to undergo a considerable reduction in mass, as small carbon clusters, especially dimers, are ejected from the tube (79); such mass loss likely contributes significantly to the plasticity of the failure mechanisms. These results also suggest that nanotubes, either single- or multiwalled, may be electrically annealed and thereby healed of large defects.

DISCUSSION

Reported stiffness and strength values of CNT bundles typically lie well below the values predicted (or observed) for isolated nanotubes. In part, this results from the relatively weak nonbonded interactions between the tubes within a bundle, which limit load transfer to the interior tubes. By modeling the load as being distributed only on the exterior of the bundle, Yu et al. (124) obtained a seemingly reasonable Young's modulus value of 1.00 TPa. However, a close examination of their stress-strain curves (see figure 2 of their paper) shows curves characterized by intermingled stretching steps with two distinct stiffness constants: one of ~2 TPa and the second of 0.3 TPa (calculated under the assumption that only the outer tubes are load bearing). All four of the bundles with reported failure strains greater than 2.1% include significant strain steps at this lower effective stiffness; the bundle with the highest reported failure strain (5.3%) has a stress-strain curve characterized entirely by this effective stiffness. This suggests there is significant load transfer into the interior of the bundle, but at various times slippage occurs perhaps at the EBID attachment to the cantilever, between the bundle and the rest of the tangled fibers in the SWCNT paper, within the bundle, or some combination thereof. The presence of this and other complications makes it difficult to extract unambiguous conclusions about properties of individual tubes from any of the fracture experiments involving bundles.

Interestingly, the as-grown bundles typically show better mechanical properties than the fabricated CNT yarns; presumably this partly results from a larger diameter in the yarns and increased defects introduced in the spinning process. Irradiation to introduce intertube bridging defects (88) may result in improvement of the tensile strength, as Kis et al. (88) observed for shear properties.

Early enthusiasm for plastic failure mechanisms for CNT fracture was fueled in part by the similarity of initial reports of failure-strain measurements of 5%–6% (122, 124) to the strain at which the stress-induced formation of SW defects is believed to become energetically favorable (~5%). Such failure mechanisms are undoubtedly important when the CNTs undergo intense irradiation or heating (146, 148, 149); however, strong evidence for plastic failure from SW transformations in any of the experiments conducted at room temperature is lacking. Indeed, nearly all the MWCNT fracture events occurred at failure strains well below those at which SW transformations are energetically favorable (much less kinetically likely). Instead, brittle failure resulting from large defects is sufficient to explain most of the experimental results, although two fracture events reported by Ding et al. (139) seem to involve plastic failure at surprisingly low failure strains and therefore remain difficult to rationalize. The preliminary results of Huang et al. (149) showing annealed, room-temperature SWCNTs fracturing at ~15% strains, albeit without fracture-stress measurements,

suggest that direct strength measurements of SWCNTs demonstrating strengths that are a substantial fraction of the theoretical peak values may soon become possible.

In comparing the WS_2 nanotube measurements with analogous data for MWCNTs, one notes that these tubes tend to fail at much larger strains, and the observed distribution of failure stresses is much more uniform. WS_2 nanotubes are less sensitive to oxidation than CNTs, and they do not have an obvious analog of an SW transformation; thus, the excellent properties observed likely result from a lower propensity for defects. The fracture strength of BN nanotubes has thus far not been directly measured experimentally; however, theoretical calculations suggest that their mechanical properties are similar to those of CNTs, whereas the tubes seem to be less sensitive to oxidation. Thus, BN nanotubes may ultimately provide a more convenient source of high-strength fiber reinforcements than CNTs.

Researchers are making rapid progress in both the direct high-resolution imaging (69) of defects and in other characterization approaches (150). Therefore, our understanding of the types and concentrations of defects that occur in nanoscale materials, the situations under which they arise, and their role in limiting fracture strength is likely to improve considerably in the near future.

SUMMARY POINTS

1. Small defects such as vacancies and SW defects reduce CNT fracture strength only modestly.
2. Relatively large defects seem to be present in all of the nanotube materials for which fracture studies have been conducted.
3. Purification schemes, especially oxidative etching, can significantly degrade the fracture strength of CNTs.
4. Irradiation-induced defects may provide a route to increasing the load transfer in CNTs.

ACKNOWLEDGMENTS

We gratefully acknowledge the grant support from the NASA University Research, Engineering, and Technology Institute on Bio Inspired Materials (BIMat) under award no. NCC-1-02037.

LITERATURE CITED

1. Ballarini R, Kayacan R, Ulm F-J, Belytschko T, Heuer AH. 2005. Biological structures mitigate catastrophic fracture through various strategies. *Int. J. Fract.* 135:187–97
2. Fantner GE, Oroudjev E, Schitter G, Golde LS, Thurner P, et al. 2006. Sacrificial bonds and hidden length: unraveling molecular mesostructures in tough materials. *Biophys. J.* 90:1411–18

3. Saito R, Dresselhaus G, Dresselhaus MS. 1998. *Physical Properties of Carbon Nanotubes*. London: Imperial College Press. 259pp.
4. Viculis LM, Mack JJ, Kaner RB. 2003. A chemical route to carbon nanoscrolls. *Science* 299:1361
5. Ruland W, Schaper AK, Hou H, Greiner A. 2003. Multi-wall carbon nanotubes with uniform chirality: evidence for scroll structures. *Carbon* 41:423–27
6. Schniepp HC, Li J-L, McAllister MJ, Sai H, Herrera-Alonso M, et al. 2006. Functionalized single graphene sheets derived from splitting graphite oxide. *J. Phys. Chem. A* 110:8535–39
7. Espinosa HD, Peng B, Prorok BC, Moldovan N, Auciello O, et al. 2003. Fracture strength of ultrananocrystalline diamond thin films: identification of Weibull parameters. *J. Appl. Phys.* 94:6076–84
8. Paci JT, Belytschko T, Schatz GC. 2005. The mechanical properties of single-crystal and ultrananocrystalline diamond: a theoretical study. *Chem. Phys. Lett.* 414:351–58
9. Wong EW, Sheehan PE, Lieber CM. 1997. Nanobeam mechanics: elasticity, strength, and toughness of nanorods and nanotubes. *Science* 277:1971–75
10. Wu B, Heidelberg A, Boland J. 2005. Mechanical properties of ultrahigh-strength gold nanowires. *Nat. Mater.* 4:525–29
11. Ding W, Calabri L, Chen X, Kohlhaas KM, Ruoff RS. 2006. Mechanics of crystalline boron nanowires. *Compos. Sci. Technol.* 66:1109–21
12. Ajayan PM, Stephan O, Redlich P, Collier C. 1995. Carbon nanotubes as removable templates for metal oxide nanocomposites and nanostructures. *Nature* 375:564–67
13. Arroyo M, Belytschko T. 2003. Nonlinear mechanical response and rippling of thick multiwalled carbon nanotubes. *Phys. Rev. Lett.* 91:215505
14. Arroyo M, Belytschko T. 2004. Finite crystal elasticity of carbon nanotubes based on the exponential Cauchy-Born rule. *Phys. Rev. B* 69:115415
15. Arroyo M, Belytschko T. 2004. Finite element methods for the nonlinear mechanics of crystalline sheets and nanotubes. *Int. J. Numer. Meth. Eng.* 59:419–56
16. Mielke SL, Troya D, Zhang S, Li J-L, Xiao S, et al. 2004. The role of vacancy defects and holes in the fracture of carbon nanotubes. *Chem. Phys. Lett.* 390:413–20
17. Abraham FF, Broughton JQ, Bernstein N, Kaxiras E. 1998. Spanning the length scales in dynamic simulation. *Comput. Phys.* 12:538–46
18. Shilkrot LE, Curtin WA, Miller RE. 2002. A coupled atomistic/continuum model of defects in solids. *J. Mech. Phys. Solids* 50:2085–306
19. Zhang S, Mielke SL, Khare R, Troya D, Ruoff RS, et al. 2005. Mechanics of defects in carbon nanotubes: atomistic and multiscale simulations. *Phys. Rev. B* 71:115403
20. Abell GC. 1985. Empirical chemical pseudopotential theory of molecular and metallic bonding. *Phys. Rev. B* 31:6184–96
21. Tersoff J. 1988. New empirical approach for the structure and energy of covalent systems. *Phys. Rev. B* 37:6991–7000
22. Tersoff J. 1988. Empirical interatomic potential for carbon, with application to amorphous carbon. *Phys. Rev. Lett.* 61:2879–82

16. Presents theoretical calculations suggesting that holes caused by purification-induced oxidative pitting are a principle source of weakness for CNTs.

23. Brenner DW. 1990. Empirical potential for hydrocarbons for use in simulating the chemical vapor deposition of diamond films. *Phys. Rev. B* 42:9458–71. Erratum. 1992. *Phys. Rev. B* 46:1948
24. Brenner DW, Shenderova OA, Harrison JA, Stuart SJ, Ni B, Sinnott SB. 2002. A second-generation reactive empirical bond order (REBO) potential energy expression for hydrocarbons. *J. Phys. Condens. Matter* 14:783–802
25. Ni B, Lee K-H, Sinnott SB. 2004. A reactive empirical bond order (REBO) potential for hydrocarbon-oxygen interactions. *J. Phys. Condens. Matter* 16:7261–75
26. Shenderova OA, Brenner DW, Omeltchenko A, Su X, Yang LH. 2000. Atomistic modeling of the fracture of polycrystalline diamond. *Phys. Rev. B* 61:3877–88
27. Belytschko T, Xiao SP, Schatz GC, Ruoff RS. 2002. Atomistic simulations of nanotube fracture. *Phys. Rev. B* 65:235430
28. Justo JF, Bazant MZ, Kaxiras E, Bulatov VV, Yip S. 1998. Interatomic potential for silicon defects and disordered phases. *Phys. Rev. B* 58:2539–50
29. Marks NA. 2001. Generalizing the environment-dependent interaction potential for carbon. *Phys. Rev. B* 63:035401
30. Van Duin ACT, Dasgupta S, Lorant F, Goddard WA III. 2001. ReaxFF: a reactive force field for hydrocarbons. *J. Phys. Chem. A* 105:9396–409
31. Pettifor DG, Oleinik II. 1999. Analytic bond-order potentials beyond Tersoff-Brenner. I. Theory. *Phys. Rev. B* 59:8487–99
32. Drautz R, Murdick DA, Nguyen-Manh D, Zhou X, Wadley HNG, Pettifor DG. 2005. Analytic bond-order potential for predicting structural trends across the *sp*-valent elements. *Phys. Rev. B* 72:144105
33. Bettinger HF. 2004. Effects of finite carbon nanotube length on sidewall addition of fluorine atom and methylene. *Org. Lett.* 6:731–35
34. Zhou Z, Steigerwald M, Hybertsen M, Brus L, Friesner RA. 2004. Electronic structure of tubular aromatic molecules derived from the metallic (5,5) armchair single wall carbon nanotube. *J. Am. Chem. Soc.* 126:3597–607
35. Chen Z, Nagase S, Hirsch A, Haddon RC, Thiel W, Schleyer PVR. 2004. Side-wall opening of single-walled carbon nanotubes (SWCNTs) by chemical modification: a critical theoretical study. *Angew. Chem. Int. Ed. Engl.* 43:1552–54
36. Fan X, Dickey EC, Eklund PC, Williams KA, Grigorian L, et al. 2000. Atomic arrangement of iodine atoms inside single-walled carbon nanotubes. *Phys. Rev. Lett.* 84:4621–24
37. Iijima S. 1991. Helical microtubules of graphitic carbon. *Nature* 354:56–58
38. Nikolaev P, Bronikowski MJ, Bradley RK, Rohmund F, Colbert DT, et al. 1999. Gas-phase catalytic growth of single-walled carbon nanotubes from carbon monoxide. *Chem. Phys. Lett.* 313:91–97
39. Wei J, Jiang B, Wu D, Wei B. 2004. Large-scale synthesis of long double-walled carbon nanotubes. *J. Phys. Chem. B* 108:8844–47
40. Kim YA, Muramatsu H, Hayashi T, Endo M, Terrones M, Dresselhaus MS. 2004. Thermal stability and structural changes of double-walled carbon nanotubes by heat treatment. *Chem. Phys. Lett.* 398:87–92

41. Muramatsu H, Hayashi T, Kim YA, Shimamoto D, Kim YJ, et al. 2005. Pore structure and oxidation stability of double-walled carbon nanotube-derived bucky paper. *Chem. Phys. Lett.* 414:444–48
42. Pan ZW, Xie SS, Chang BH, Wang CY, Lu L, et al. 1998. Very long carbon nanotubes. *Nature* 394:631–32
43. Andrews R, Jacques D, Rao AM, Derbyshire F, Qian D, et al. 1999. Continuous production of aligned carbon nanotubes: a step closer to commercial realization. *Chem. Phys. Lett.* 303:467–74
44. Zheng LX, O'Connell MJ, Doorn SK, Liao XZ, Zhao YH, et al. 2004. Ultralong single-wall carbon nanotubes. *Nat. Mater.* 3:673–76
45. Gao G, Cagin T, Goddard WA III. 1998. Energetics, structure, mechanical and vibrational properties of single-walled carbon nanotubes. *Nanotechnology* 9:184–91
46. Zhang S, Khare R, Belytschko T, Hsia KJ, Mielke SL, Schatz GC. 2006. Transition states and minimum energy pathways for the collapse of carbon nanotubes. *Phys. Rev. B* 73:075423
47. Ogata S, Shibutani Y. 2003. Ideal tensile strength and band gap of single-walled carbon nanotubes. *Phys. Rev. B* 68:165409
48. Ozaki T, Iwasa Y, Mitani T. 2000. Stiffness of single-walled carbon nanotubes under large strain. *Phys. Rev. Lett.* 84:1712–15
49. Troya D, Mielke SL, Schatz GC. 2003. Carbon nanotube fracture—differences between quantum mechanical mechanisms and those of empirical potentials. *Chem. Phys. Lett.* 382:133–41
50. Dumitrica T, Belytschko T, Yakobson BI. 2003. Bond-breaking bifurcation states in carbon nanotube fracture. *J. Chem. Phys.* 118:9485–88
51. Sanchez-Portal D, Artacho E, Soler JM, Rubio A, Ordejon P. 1999. Ab initio structural, elastic, and vibrational properties of carbon nanotubes. *Phys. Rev. B* 59:12678–88
52. Kudin KN, Scuseria GE, Yakobson BI. 2001. C_2F, BN, and C nanoshell elasticity from ab initio computations. *Phys. Rev. B* 64:235406
53. Chopra NG, Luyken RJ, Cherrey K, Crespi VH, Cohen ML, et al. 1995. Boron nitride nanotubes. *Science* 269:966–67
54. Tenne R, Margulis L, Genut M, Hodes G. 1992. Polyhedral and cylindrical structures of tungsten disulphide. *Nature* 360:444–46
55. Rothschild A, Popovitz-Biro R, Lourie O, Tenne R. 2000. Morphology of multiwall WS_2 nanotubes. *J. Phys. Chem. B* 104:8976–81
56. Margulis L, Salitra G, Tenne R, Talianker M. 1993. Nested fullerene-like structures. *Nature* 365:113–14
57. Seifert G, Terrones H, Terrones M, Jungnickel G, Frauenheim T. 2000. Structure and electronic properties of MoS_2 nanotubes. *Phys. Rev. Lett.* 85:146–49
58. Bengu E, Marks LD. 2001. Single-walled BN nanostructures. *Phys. Rev. Lett.* 86:2385–87
59. Weng-Sieh Z, Cherrey K, Chopra NG, Blase X, Miyamoto Y, et al. 1995. Synthesis of $B_xC_yN_z$ nanotubules. *Phys. Rev. B* 51:11229–32
60. Han W-Q, Mickelson W, Cumings J, Zettl A. 2002. Transformation of $B_xC_yN_z$ nanotubes to pure BN nanotubes. *Appl. Phys. Lett.* 81:1110–12

61. Han W, Bando Y, Kurashima K, Sato T. 1998. Synthesis of boron nitride nanotubes from carbon nanotubes by a substitution reaction. *Appl. Phys. Lett.* 73:3085–87
62. Chen H, Chen Y, Yu J, Williams JS. 2006. Purification of boron nitride nanotubes. *Chem. Phys. Lett.* 425:315–19
63. Stone AJ, Wales DJ. 1986. Theoretical studies of icosahedral C_{60} and some related species. *Chem. Phys. Lett.* 128:501–3

64. Discusses plastic failure from dislocation creation by SW transformations.

64. Nardelli MB, Yakobson BI, Bernholc J. 1998. Mechanism of strain release in carbon nanotubes. *Phys. Rev. B* 57: R4277–80
65. Zhao Q, Nardelli MB, Bernholc J. 2002. Ultimate strength of carbon nanotubes: a theoretical study. *Phys. Rev. B* 65:144105
66. Zhang P, Lammert PE, Crespi VH. 1998. Plastic deformations of carbon nanotubes. *Phys. Rev. Lett.* 81:5346–49
67. Yakobson BI. 1998. Mechanical relaxation and "intramolecular plasticity" in carbon nanotubes. *Appl. Phys. Lett.* 72:918–20
68. Nardelli MB, Yakobson BI, Bernholc J. 1998. Brittle and ductile behavior in carbon nanotubes. *Phys. Rev. Lett.* 81:4656–59

69. Demonstrates state-of-the-art imaging of defects.

69. Hashimoto A, Suenaga K, Gloter A, Urita K, Iijima S. 2004. Direct evidence for atomic defects in graphene layers. *Nature* 430:870–73
70. Samsonidze GG, Samsonidze GG, Yakobson BI. 2002. Kinetic theory of symmetry-dependent strength in carbon nanotubes. *Phys. Rev. Lett.* 88:065501
71. Dumitrica T, Yakobson BI. 2004. Strain-rate and temperature dependent plastic yield in carbon nanotubes from ab initio calculations. *Appl. Phys. Lett.* 84:2775–77
72. Dumitrica T, Hua M, Yakobson BI. 2006. Symmetry-, time-, and temperature-dependent strength of carbon nanotubes. *Proc. Natl. Acad. Sci. USA* 103:6105–9
73. Zhang P, Crespi VH. 2000. Plastic deformations of boron-nitride nanotubes: an unexpected weakness. *Phys. Rev. B* 62:11050–503
74. Bettinger HF, Dumitrica T, Scuseria GE, Yakobson BI. 2002. Mechanically induced defects and strength of BN nanotubes. *Phys. Rev. B* 65:041406
75. Dumitrica T, Yakobson BI. 2005. Rate theory of yield in boron nitride nanotubes. *Phys. Rev. B* 72:035418
76. Wei C, Cho K, Srivastava D. 2003. Tensile strength of carbon nanotubes under realistic temperature and strain rate. *Phys. Rev. B* 67:115407
77. Wei C, Cho K, Srivastava D. 2003. Tensile yielding of multiwall carbon nanotubes. *Appl. Phys. Lett.* 82:2512–14
78. Bettinger HF. 2005. The reactivity of defects at the sidewalls of single-walled carbon nanotubes: the Stone-Wales defect. *J. Phys. Chem. B* 109:6922–24
79. Ewels CP, Heggie MI, Briddon PR. 2002. Adatoms and nanoengineering of carbon. *Chem. Phys. Lett.* 351:178–82
80. Jensen P, Gale J, Blase X. 2002. Catalysis of nanotube plasticity under tensile strain. *Phys. Rev. B* 66:193403

81. Shows that ad-dimers provide another source for dislocations.

81. Orlikowski D, Nardelli MB, Bernholc J, Roland C. 1999. Ad-dimers on strained carbon nanotubes: a new route for quantum dot formation? *Phys. Rev. Lett.* 83:4132–35

82. Orlikowski D, Nardelli MB, Bernholc J, Roland C. 2000. Theoretical STM signatures and transport properties of native defects in carbon nanotubes. *Phys. Rev. B* 61:14194–203
83. Sternberg M, Curtiss LA, Gruen DM, Kedziora G, Horner DA, et al. 2006. Carbon ad-dimer defects in carbon nanotubes. *Phys. Rev. Lett.* 96:075506
84. Nordund K, Keinonen J, Mattila T. 1996. Formation of ion irradiation induced small-scale defects on graphite surfaces. *Phys. Rev. Lett.* 77:699–702
85. Ajayan PM, Ravikumar V, Charlier J-C. 1998. Surface reconstructions and dimensional changes in single-walled carbon nanotubes. *Phys. Rev. Lett.* 81:1437–40
86. Krasheninnikov AV, Nordlund K, Sirvio M, Salonen E, Keinonen J. 2001. Formation of ion-irradiation-induced atomic-scale defects on walls of carbon nanotubes. *Phys. Rev. B* 63:245405
87. Telling RH, Ewels CP, El-Barbary AA, Heggie MI. 2003. Wigner defects bridge the graphite gap. *Nat. Mater.* 2:333–37
88. Kis A, Csanyi G, Saletat J-P, Lee T-N, Couteau E, et al. 2004. Reinforcement of single-walled carbon nanotube bundles by intertube bridging. *Nat. Mater.* 3:153–57
89. Sammalkorpi M, Krasheninnikov A, Kuronen A, Nordlund K, Kaski K. 2004. Mechanical properties of carbon nanotubes with vacancies and related defects. *Phys. Rev. B* 70:245416. Erratum. 2005. *Phys. Rev. B* 71:169906
90. Krasheninnikov AV, Banhart F, Li JX, Foster AS, Nieminen RM. 2005. Stability of carbon nanotubes under electron irradiation: role of tube diameter and chirality. *Phys. Rev. B* 72:125428
91. Krasheninnikov AV, Nordlund K, Keinonen J. 2002. Production of defects in supported carbon nanotubes under ion irradiation. *Phys. Rev. B* 65:165423
92. Crespi VH, Chopra NG, Cohen ML, Zettl A, Louie SG. 1996. Anisotropic electron-beam damage and the collapse of carbon nanotubes. *Phys. Rev. B* 54:5927–31
93. Terrones M, Terrones H, Banhart F, Charlier J-C, Ajayan PM. 2000. Coalescence of single-walled carbon nanotubes. *Science* 188:1226–29
94. Kang HS. 2006. Theoretical study of boron nitride nanotubes with defects in nitrogen-rich synthesis. *J. Phys. Chem. B* 110:4621–28
95. Schmidt TM, Baierle RJ, Piquini P, Fazzio A. 2003. Theoretical study of native defects in BN nanotubes. *Phys. Rev. B* 67:113407
96. Yang RT, Wong C. 1981. Mechanism of single-layer graphite oxidation: evaluation by electron microscopy. *Science* 214:437–38
97. Yang RT, Wong C. 1981. Kinetics and mechanism of oxidation of basal plane on graphite. *J. Chem. Phys.* 75:4471–76
98. Stevens F, Kolodny LA, Beebe TP Jr. 1998. Kinetics of graphite oxidation: monolayer and multilayer etch pits in HOPG studied by STM. *J. Phys. Chem. B* 102:10799–804
99. Lee SM, Lee YH, Hwang YG, Hahn JR, Kang H. 1999. Defect-induced oxidation of graphite. *Phys. Rev. Lett.* 82:217–20
100. Ciraci S, Dag S, Yildirim T, Gulseren O, Senger RT. 2004. Functionalized carbon nanotubes and device applications. *J. Phys. Condens. Matter* 16: R901–60

88. Demonstrates how irradiation-induced defects can be used to increase the mechanical properties of CNTs.

101. Bettinger HF. 2003. Experimental and computational investigations of the properties of fluorinated single-walled carbon nanotubes. *Chemphyschem* 4:1283–89
102. Zhang Y-F, Liu Z-F. 2006. Pressure induced reactivity change on the sidewall of a carbon nanotube: a case study on the addition of singlet O_2. *Carbon* 44:928–38
103. Srivastava D, Brenner DW, Schall JD, Ausman KD, Yu MF, Ruoff RS. 1999. Predictions of enhanced chemical reactivity at regions of local conformational strain on carbon nanotubes: kinky chemistry. *J. Phys. Chem. B* 103:4330–37
104. Banerjee S, Wong SS. 2004. Demonstration of diameter-selective reactivity in the sidewall ozonation of SWNTs by resonance Raman spectroscopy. *Nano Lett.* 4:1445–50
105. Zhang J, Zou H, Qing Q, Yang Y, Li Q, et al. 2003. Effect of chemical oxidation on the structure of single-walled carbon nanotubes. *J. Phys. Chem. B* 107:3712–18
106. Mickelson ET, Huffman CB, Rinzler AG, Smalley RE, Hauge RH, Margrave JL. 1998. Fluorination of single-wall carbon nanotubes. *Chem. Phys. Lett.* 296:188–94
107. Kelly KF, Chiang IW, Mickelson ET, Hauge RH, Margrave JL, et al. 1999. Insight into the mechanism of sidewall functionalization of single-walled nanotubes: an STM study. *Chem. Phys. Lett.* 313:445–50
108. Mickelson ET, Chiang IW, Zimmerman JL, Boul PJ, Lozano J, et al. 1999. Solvation of fluorinated single-wall carbon nanotubes in alcohol solvents. *J. Phys. Chem. B* 103:4318–22
109. Khare BN, Meyyappan M, Kralj J, Wilhite P, Sisay M, et al. 2002. A glow-discharge approach for functionalization of carbon nanotubes. *Appl. Phys. Lett.* 81:5237–39
110. Plank NOV, Jiang L, Cheung R. 2003. Fluorination of carbon nanotubes in CF_4 plasma. *Appl. Phys. Lett.* 83:2426–28
111. Valentini L, Puglia D, Armentano I, Kenny JM. 2005. Sidewall functionalization of single-walled carbon nanotubes through CF_4 plasma treatment and subsequent reaction with aliphatic amines. *Chem. Phys. Lett.* 403:385–89
112. Xu Y-Q, Peng H, Hauge RH, Smalley RE. 2005. Controlled multistep purification of single-walled carbon nanotubes. *Nano Lett.* 5:163–68
113. Wiltshire JG, Khlobystov AN, Li LJ, Lyapin SG, Briggs GAD, Nicholas RJ. 2004. Comparative studies on acid and thermal based selective purification of HiPCO produced single-walled carbon nanotubes. *Chem. Phys. Lett.* 386:239–43
114. Rinzler AG, Liu J, Dai H, Nikolaev P, Huffman CB, et al. 1998. Large-scale purification of single-wall carbon nanotubes: process, product, and characterization. *Appl. Phys. A* 67:29–37
115. Haddon RC, Sippel J, Rinzler AG, Papadimitrakopoulos F. 2004. Purification and separation of carbon nanotubes. *MRS Bull.* 29:252–59
116. Liu J, Rinzler AG, Dai H, Hafner JH, Bradley RK, et al. 1998. Fullerene pipes. *Science* 280:1253–56

117. Vivekchand SRC, Govindaraj A, Seikh MM, Rao CNR. 2004. New method of purification of carbon nanotubes based on hydrogen treatment. *J. Phys. Chem. B* 108:6935–37
118. Bom D, Andrews R, Jacques D, Anthony J, Chen B, et al. 2002. Thermogravimetric analysis of the oxidation of multiwalled carbon nanotubes: evidence for the role of defect sites in carbon nanotube chemistry. *Nano Lett.* 2:615–19
119. Park KC, Hayashi T, Tomiyasu H, Endo M, Dresselhaus MS. 2004. Progressive and invasive functionalization of carbon nanotube sidewalls by diluted nitric acid under supercritical conditions. *J. Mater. Chem*. 15:407–11
120. Wagner HD, Lourie O, Feldman Y, Tenne R. 1998. Stress-induced fragmentation of multiwall carbon nanotubes in a polymer matrix. *Appl. Phys. Lett*. 72:188–90
121. Pan ZW, Xie SS, Lu L, Chang BH, Sun LF, et al. 1998. Tensile tests of ropes of very long aligned multiwall carbon nanotubes. *Appl. Phys. Lett.* 74:3152–54
122. Walters DA, Ericson LM, Casavant MJ, Liu J, Colbert DT, et al. 1999. Elastic strain of freely suspended single-wall carbon nanotube ropes. *Appl. Phys. Lett.* 74:3803–5
123. Thess A, Lee R, Nikolaev P, Dai H, Petit P, et al. 1996. Crystalline ropes of metallic carbon nanotubes. *Science* 273:483–87
124. Yu M-F, Files BS, Arepalli S, Ruoff RS. 2000. Tensile loading of ropes of single wall canbon nanotubes and their mechanical properties. *Phys. Rev. Lett*. 84:5552–55
125. Li C, Ruoff RS, Chou T-W. 2005. Modeling of carbon nanotube clamping in tensile tests. *Compos. Sci. Technol*. 65:2407–15
126. Li F, Cheng HM, Bai S, Su G, Dresselhaus MS. 2000. Tensile strength of single-walled carbon nanotubes directly measured from their macroscopic ropes. *Appl. Phys. Lett*. 77:3161–63
127. Cheng HM, Li F, Sun X, Brown SDM, Pimenta MA, et al. 1998. Bulk morphology and diameter distribution of single-walled carbon nanotubes synthesized by catalytic decomposition of hydrocarbons. *Chem. Phys. Lett.* 289:602–10
128. Cooper CA, Cohen SR, Barber AH, Wagner HD. 2002. Detachment of nanotubes from a polymer matrix. *Appl. Phys. Lett*. 81:3873–75
129. Li Y, Wang K, Wei J, Gu Z, Wang Z, et al. 2005. Tensile properties of long aligned double-walled carbon nanotube strands. *Carbon* 43:31–35
130. Jiang K, Li Q, Fan S. 2002. Spinning continuous carbon nanotube yarns. *Nature* 419:801
131. Zhang M, Atkinson KR, Baughman RH. 2002. Multifunctional carbon nanotube yarns by downsizing an ancient technology. *Science* 306:1358–61
132. Ericson LM, Fan H, Peng H, Davis VA, Zhou W, et al. 2004. Macroscopic, neat, single-walled carbon nanotube fibers. *Science* 305:1447–50
133. Yu M-F, Lourie O, Dyer MJ, Moloni K, Kelly TF, Ruoff RS. 2000. Strength and breaking mechanism of multiwalled carbon nanotubes under tensile load. *Science* 287:637–40
134. Colbert DT, Zhang J, McClure SM, Nikolaev P, Chen Z, et al. 1994. Growth and sintering of fullerene nanotubes. *Science* 266:1218–22

133. Presents the first MWCNT fracture experiment.

135. Yu M-F, Ruoff RS, Yakobson BI. 2001. Controlled sliding and pullout of nested shells in individual multiwalled carbon nanotubes. *J. Phys. Chem. B* 104:8764–67

136. Demczyk BG, Wang YM, Cumings J, Hetman M, Han W, et al. 2002. Direct mechanical measurement of the tensile strength and elastic modulus of multiwalled carbon nanotubes. *Mater. Sci. Eng. A* 334:173–78

137. Redlich P, Loeffler J, Ajayan PM, Bill J, Aldinger F, Ruhle M. 1996. B-C-N nanotubes and boron doping of carbon nanotubes. *Chem. Phys. Lett.* 260:465–70

138. Endo M, Muramatsu H, Hayashi T, Kim Y-A, Van Lier G, et al. 2005. Atomic nanotube welders: boron interstitials triggering connections in double-walled carbon nanotubes. *Nano Lett.* 5:1099–105

139. Presents an MWCNT fracture experiment with unpurified arc-grown nanotubes.

139. Ding W, Calabri L, Kohlhaas KM, Chen X, Dikin DA, Ruoff RS. 2006. Modulus, fracture strength, and brittle vs plastic response of the outer shell of arc-grown multi-walled carbon nanotubes. *Exp. Mech.* In press

140. Presents an MWCNT fracture study with CVD-grown tubes.

140. Barber AH, Andrews R, Schadler LS, Wagner HD. 2005. On the tensile strength distribution of multiwalled carbon nanotubes. *Appl. Phys. Lett.* 87:203106

141. Barber AH, Kaplan-Ashiri I, Cohen SR, Tenne R, Wagner HD. 2005. Stochastic strength of nanotubes: an appraisal of available data. *Compos. Sci. Technol.* 65:2380–84

142. Presents a fracture study with multiwalled tungsten disulfide nanotubes.

142. Kaplan-Ashiri I, Cohen SR, Gartsman K, Ivanovskaya V, Heine T, et al. 2005. On the mechanical behavior of WS_2 nanotubes under axial tension and compression. *Proc. Natl. Acad. Sci. USA* 103:523–28

143. Kaplan-Ashiri I, Cohen SR, Gartsman K, Rosentsveig R, Seifert G, Tenne R. 2004. Mechanical behavior of individual WS_2 nanotubes. *J. Mater. Res.* 19:454–59

144. Hong BH, Small JP, Purewal MS, Mullokandov A, Sfeir MY, et al. 2005. Extracting subnanometer single shells from ultralong multiwalled carbon nanotubes. *Proc. Natl. Acad. Sci. USA* 102:14155–58

145. Hong BH, Lee JY, Beetz T, Zhu Y, Kim P, Kim KS. 2005. Quasi-continuous growth of ultralong carbon nanotube arrays. *J. Am. Chem. Soc.* 127:15336–37

146. Troiani HE, Miki-Yoshida M, Camacho-Bragado GA, Marques MAL, Rubio A, et al. 2003. Direct observation of the mechanical properties of single-walled carbon nanotubes and their junctions at the atomic level. *Nano Lett.* 3:751–55

147. Yakobson BI, Cambell MP, Brabec CJ, Bernholc J. 1997. High strain rate fracture and C-chain unraveling in carbon nanotubes. *Comput. Mater. Sci.* 8:341–48

148. Bozovic D, Bockrath M, Hafner JH, Lieber CM, Park H, Tinkham M. 2003. Plastic deformations in mechanically strained single-walled carbon nanotubes. *Phys. Rev. B* 67:033407

149. Hints at fracture of cold annealed SWCNTs at ~15% strain.

149. Huang JY, Chen S, Wang ZQ, Kemp K, Wang YM, et al. 2006. Superplastic carbon nanotubes: Conditions have been discovered that allow extensive deformation of rigid single-walled nanotubes. *Nature* 439:281

150. Fan Y, Burghard M, Kern K. 2002. Chemical defect decoration of carbon nanotubes. *Adv. Mater.* 14:130–33

RELATED RESOURCES

Banhart F. 1999. Irradiation effects in carbon nanostructures. *Rep. Prog. Phys.* 62:1181–221

Bernholc J, Brenner D, Nardelli MB, Meunier V, Roland C. 2002. Mechanical and electrical properties of nanotubes. *Annu. Rev. Mater. Res.* 32:347–75

Qian D, Wagner GJ, Liu WK, Yu M-F, Ruoff RS. 2002. Mechanics of carbon nanotubes. *Appl. Mech. Rev.* 55:495–533

Sinnott SB. 2002. Chemical functionalization of carbon nanotubes. 2002. *J. Nanosci. Nanotechnol.* 2:113–23

Tasis D, Tagmatarchis N, Bianco A, Prato M. 2006. Chemistry of carbon nanotubes. *Chem. Rev.* 106:1105–36

Terrones M. 2004. Carbon nanotubes: synthesis and properties, electronic devices and other emerging applications. *Int. Mater. Rev.* 49:325–77

Annual Review of
Physical Chemistry

Volume 58, 2007

Contents

Frontispiece
C. Bradley Moore xvi

A Spectroscopist's View of Energy States, Energy Transfers, and Chemical Reactions
C. Bradley Moore 1

Stochastic Simulation of Chemical Kinetics
Daniel T. Gillespie 35

Protein-Folding Dynamics: Overview of Molecular Simulation Techniques
Harold A. Scheraga, Mey Khalili, and Adam Liwo 57

Density-Functional Theory for Complex Fluids
Jianzhong Wu and Zhidong Li 85

Phosphorylation Energy Hypothesis: Open Chemical Systems and Their Biological Functions
Hong Qian 113

Theoretical Studies of Photoinduced Electron Transfer in Dye-Sensitized TiO_2
Walter R. Duncan and Oleg V. Prezhdo 143

Nanoscale Fracture Mechanics
Steven L. Mielke, Ted Belytschko, and George C. Schatz 185

Modeling Self-Assembly and Phase Behavior in Complex Mixtures
Anna C. Balazs 211

Theory of Structural Glasses and Supercooled Liquids
Vassiliy Lubchenko and Peter G. Wolynes 235

Localized Surface Plasmon Resonance Spectroscopy and Sensing
Katherine A. Willets and Richard P. Van Duyne 267

Copper and the Prion Protein: Methods, Structures, Function, and Disease
Glenn L. Millhauser 299

Aging of Organic Aerosol: Bridging the Gap Between Laboratory and Field Studies
Yinon Rudich, Neil M. Donahue, and Thomas F. Mentel 321

Molecular Motion at Soft and Hard Interfaces: From Phospholipid Bilayers to Polymers and Lubricants
Sung Chul Bae and Steve Granick 353

Molecular Architectonic on Metal Surfaces
Johannes V. Barth 375

Highly Fluorescent Noble-Metal Quantum Dots
Jie Zheng, Philip R. Nicovich, and Robert M. Dickson 409

State-to-State Dynamics of Elementary Bimolecular Reactions
Xueming Yang 433

Femtosecond Stimulated Raman Spectroscopy
Philipp Kukura, David W. McCamant, and Richard A. Mathies 461

Single-Molecule Probing of Adsorption and Diffusion on Silica Surfaces
Mary J. Wirth and Michael A. Legg 489

Intermolecular Interactions in Biomolecular Systems Examined by Mass Spectrometry
Thomas Wyttenbach and Michael T. Bowers 511

Measurement of Single-Molecule Conductance
Fang Chen, Joshua Hihath, Zhifeng Huang, Xiulan Li, and N.J. Tao 535

Structure and Dynamics of Conjugated Polymers in Liquid Crystalline Solvents
P.F. Barbara, W.-S. Chang, S. Link, G.D. Scholes, and Arun Yethiraj 565

Gas-Phase Spectroscopy of Biomolecular Building Blocks
Mattanjah S. de Vries and Pavel Hobza 585

Isomerization Through Conical Intersections
Benjamin G. Levine and Todd J. Martínez 613

Spectral and Dynamical Properties of Multiexcitons in Semiconductor Nanocrystals
Victor I. Klimov 635

Molecular Motors: A Theorist's Perspective
Anatoly B. Kolomeisky and Michael E. Fisher 675

Bending Mechanics and Molecular Organization in Biological Membranes
Jay T. Groves 697

Exciton Photophysics of Carbon Nanotubes
Mildred S. Dresselhaus, Gene Dresselhaus, Riichiro Saito, and Ado Jorio 719